ESI

Three-dimensional interconnected V_6O_{13} nest with V^{5+}-rich state for ultrahigh Zn ion storage

Pingge He[a], Jiahao Liu[a], Xudong Zhao[a], Zhengping Ding [b], Peng Gao [b, c], Li-Zhen Fan [a,*]

[a] Beijing Advanced Innovation Center for Materials Genome Engineering, Institute of Advanced Materials and Technology, University of Science and Technology Beijing, Beijing 100083, China
[b] International Center for Quantum Materials, Electron Microscopy Laboratory, School of Physics, Peking University, Beijing 100871, China.
[c] Collaborative Innovation Centre of Quantum Matter, Beijing 100871, China

Experimental Details

The pre-treatment of carbon cloth: Firstly, the carbon clothes are cleaned using acetone and distilled water under ultrasonic condition for 10 min. The, the carbon clothes are immersed into a solution of 3M H_3PO_4 (85%) under a temperature of 60°C for overnight. Finally, the treated carbon clothes are washed with distilled water and in vacuum overnight.

The preparation of deposited-Zn on carbon cloth electrode: The deposited-Zn on carbon cloth is prepared by a facile electrochemical deposition method using two-electrode setup. In detail, the Zn plate is used as counter electrode, pre-treated carbon cloth is used as working electrode and 1 M $ZnSO_4$ is used as electrolyte. Electroplating is conducted at 5 mA·cm^{-2} for 1800 s using an electrochemical workstation (CHI 760D, Chenhua).

The assembly of flexible Zn-ion battery: First, the $ZnSO_4$-PVA gel electrolyte was prepared by mixing 2.15 g $ZnSO_4$•$7H_2O$ with deionized water (15 mL), and then adding 1.5 g PVA powder (molecular weight 89,000-98,000, 99% hydrolyzed, Sigma-Aldrich). The mixture was heated steadily from room temperature to approx. 85 °C under vigorous stirring until the solution became clear and thoroughly mixed. Then, a piece of V_6O_{13}/CC cathode and a piece of Zn/CC anode were immersed in the hot dilute polymer electrolyte solution. The dilute solution soaked and penetrated the porous electrodes well and formed a coating layer on the surface of the electrodes. The electrodes with the electrolyte solution coating on were placed in a fume hood at room temperature to evaporate the excess water. After the (0.5M) $ZnSO_4$-PVA became solidified, the two electrodes were tightly pressed together into one integrated unit. The $ZnSO_4$-PVA gel is used as both electrolyte and separator.

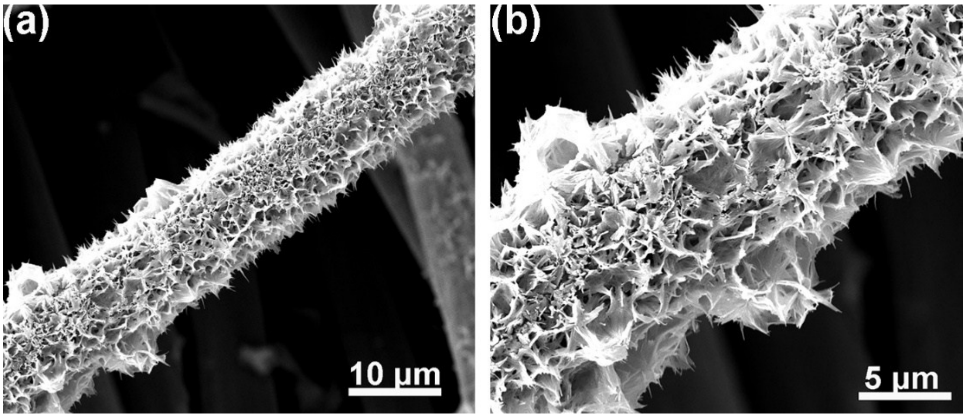

Fig. S1. SEM images of V_6O_{13} nest on CC before calcining: (a) at a low magnification; (b) at a high magnification.

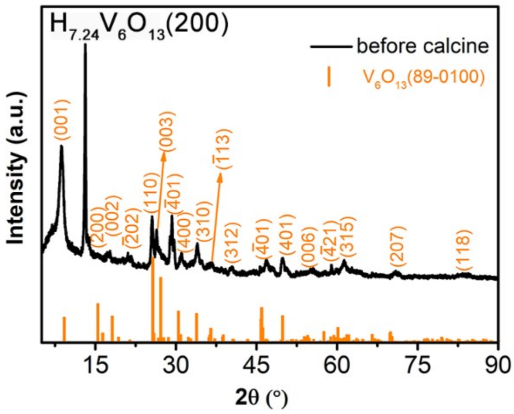

Fig. S2. XRD of V_6O_{13} powder before calcining

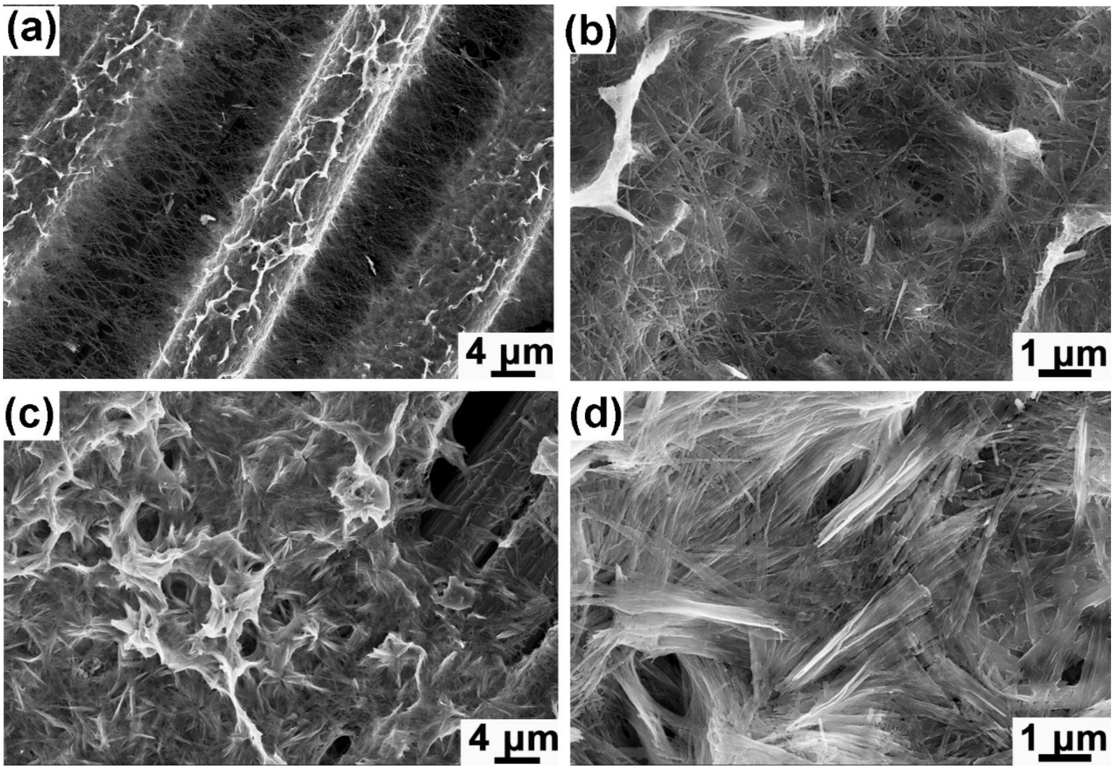

Fig. S3. SEM images of V_6O_{13} nests prepared under different hydrothermal durations: 2 h (a) at a low magnification and (b) at a high magnification. 10 h (c) at a low magnification and (d) at a high magnification.

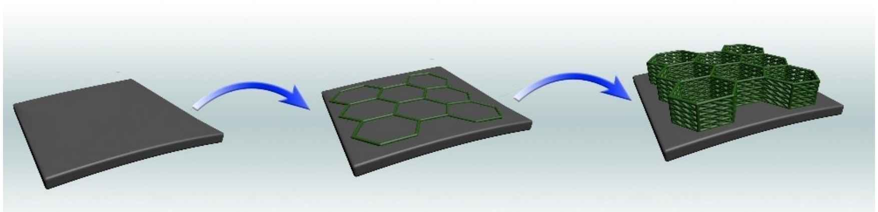

Fig. S4. Schematic of the formation process of 3D V_6O_{13} nest-like structure on CC surface.

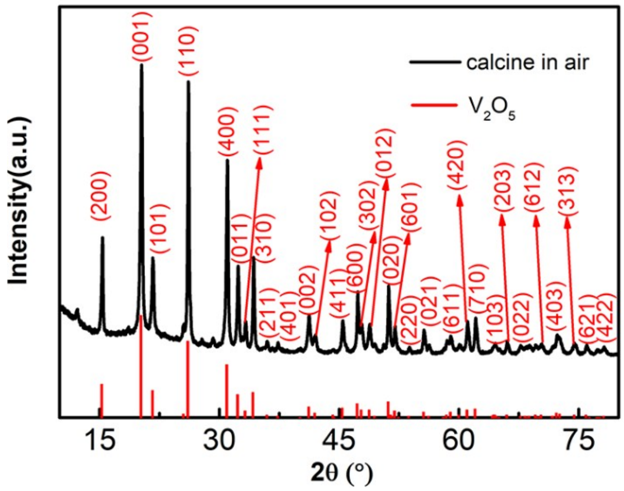

Fig. S5. XRD of products calcined in the air.

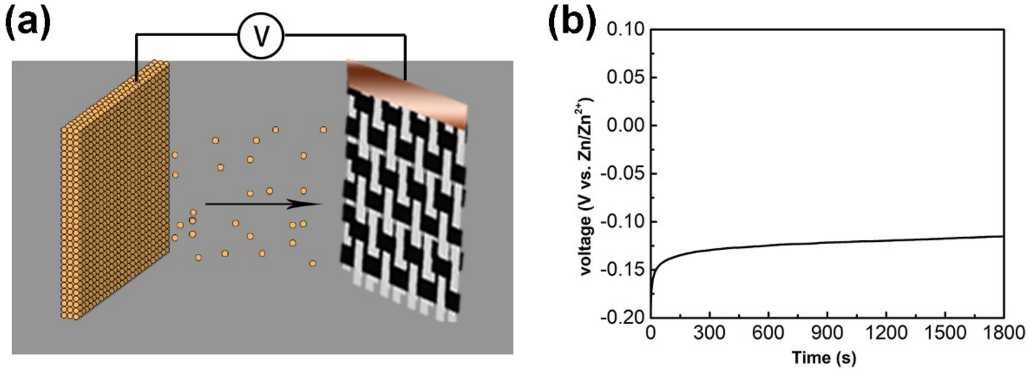

Fig. S6. Electrodeposition of Zn on CC: (a) Schematic illustration. (b) Current variation as a function of time.

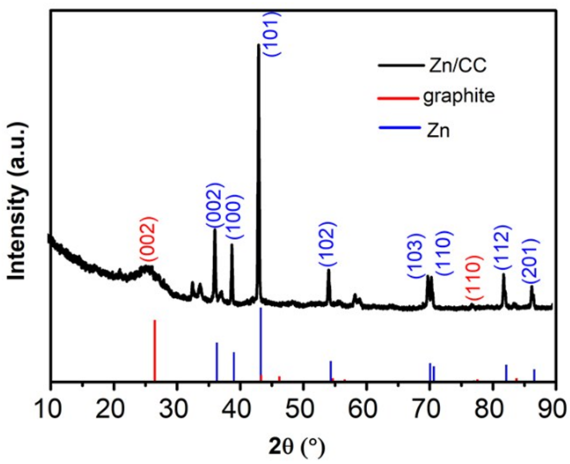

Fig. S7. XRD of Zn electrodeposited on CC.

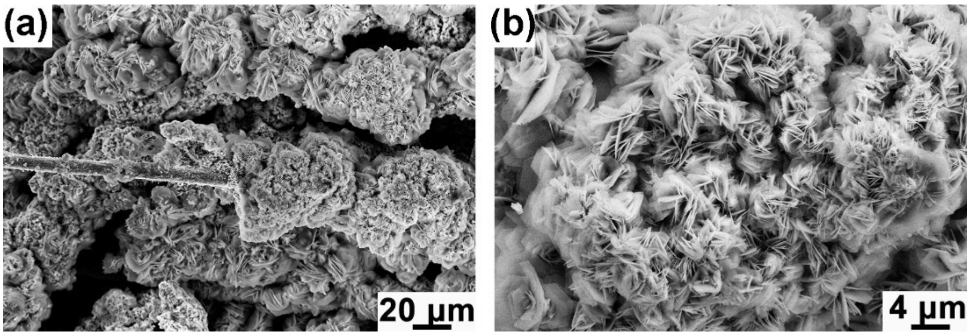

Fig. S8. SEM images of Zn electrodeposited on CC for 60 min: (a) at a low magnification. (b) at a high magnification.

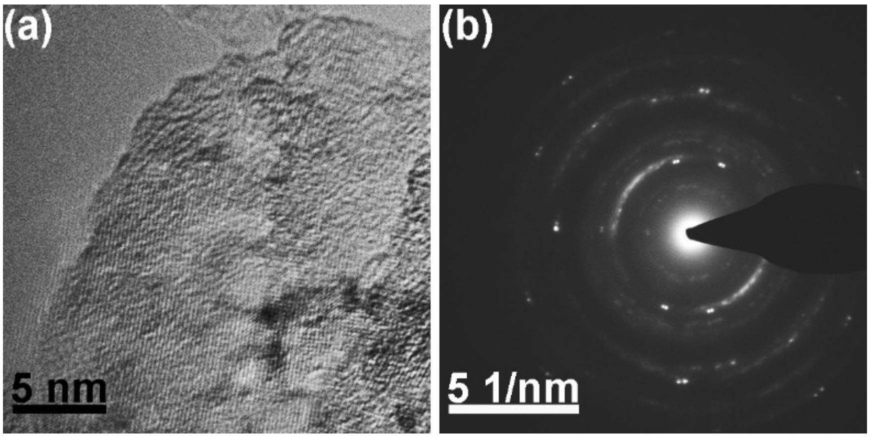

Fig. S9. (a) HRTEM of V_6O_{13} nanoneedles. (b) Corresponding selected area electron diffraction.

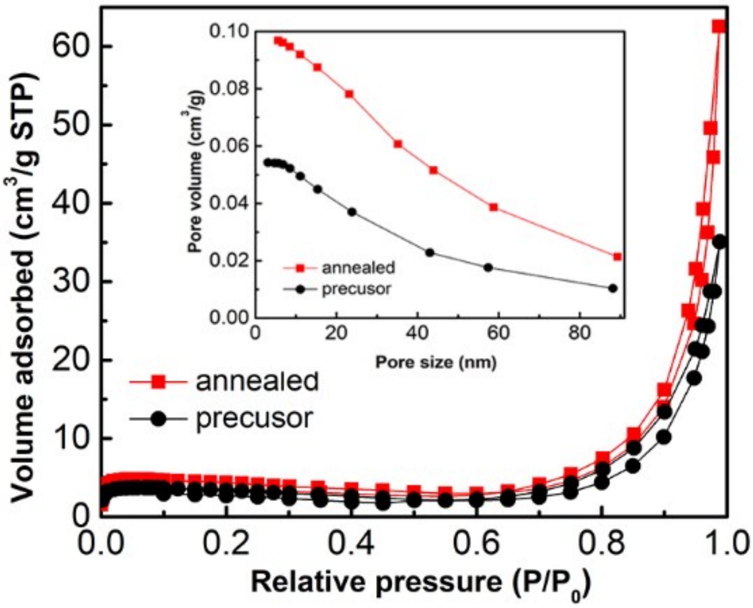

Fig. S10. N_2 adsorption and desorption curves of V_6O_{13} before and after calcining, and the inset shows the BJH pore size distribution curve.

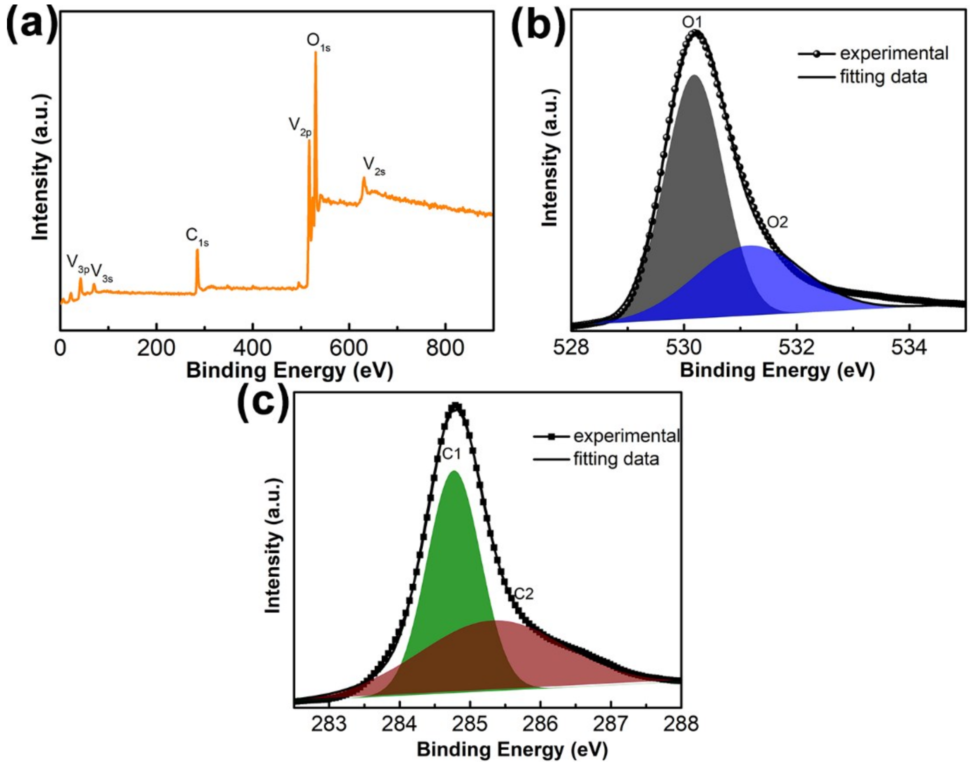

Fig. S11. XPS results of V_6O_{13}/CC: (a) full-scan spectrum; (b) O 1s; (c) C 1s.

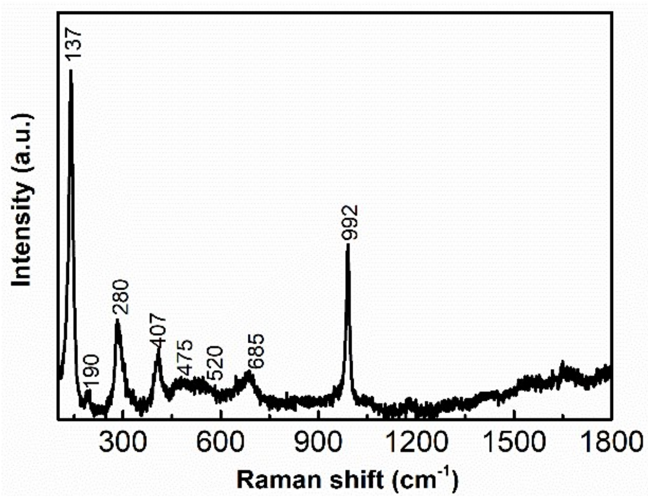

Fig. S12. Raman spectrum of bare V_6O_{13} powder.

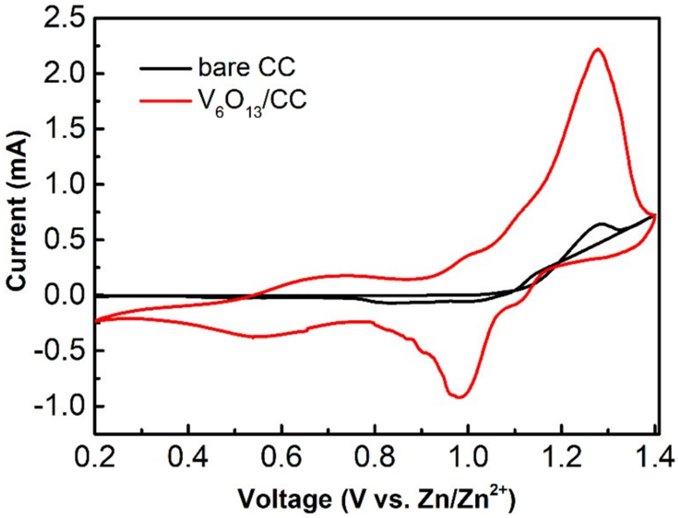

Fig. S13. Comparative CV curves of bare CC and V_6O_{13}/CC electrodes in 3M $ZnSO_4$ at a scan rate of 0.6 mV s^{-1}.

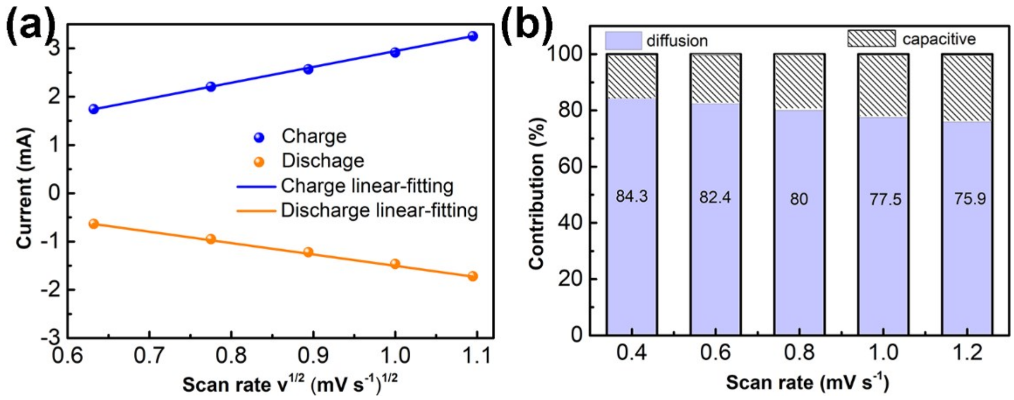

Fig. S14. The calculated diffusion contribution for V_6O_{13}/CC cathodes at different scan rates.

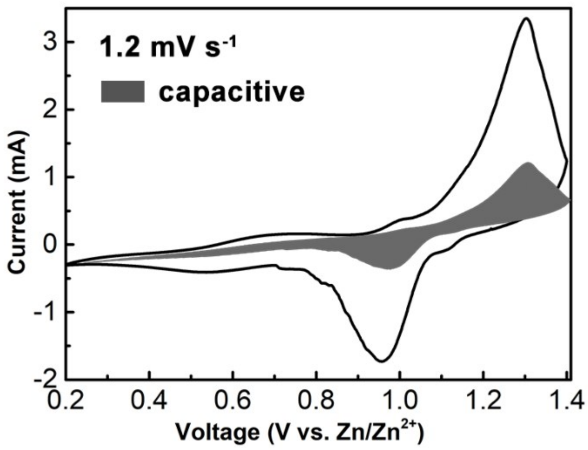

Fig. S15. Fitted CV curves suggesting the calculated capacitive contribution for V^{5+}-rich V_6O_{13}/CC cathodes at a scan rate of 1.2 mV s^{-1}.

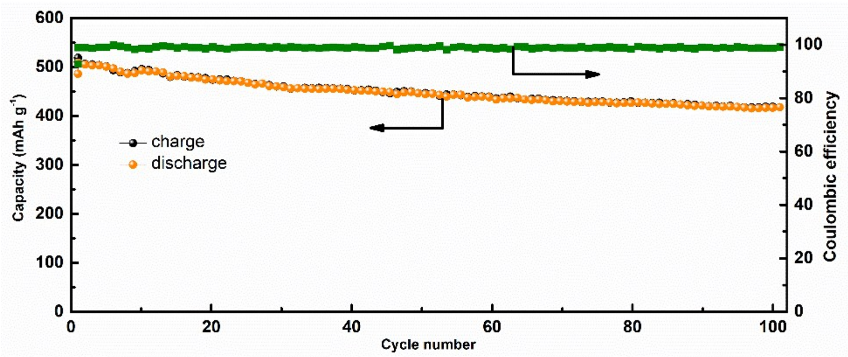

Fig. S16. Cyclic stability of V^{5+}-rich V_6O_{13}/CC electrodes at 500 mA g^{-1} over 100 cycles.

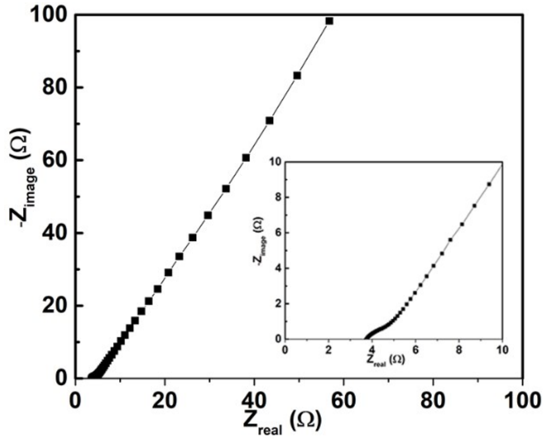

Fig. S17. Nyquist plots of well-balanced V_6O_{13} cathode (the inset shows the magnified EIS image at the high-frequency region).

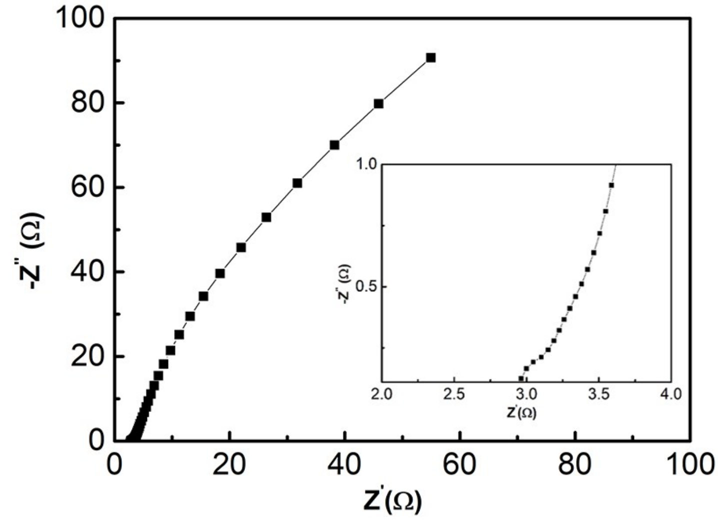

Fig. S18. Nyquist plots (the inset shows the magnified EIS image at the high-frequency region).

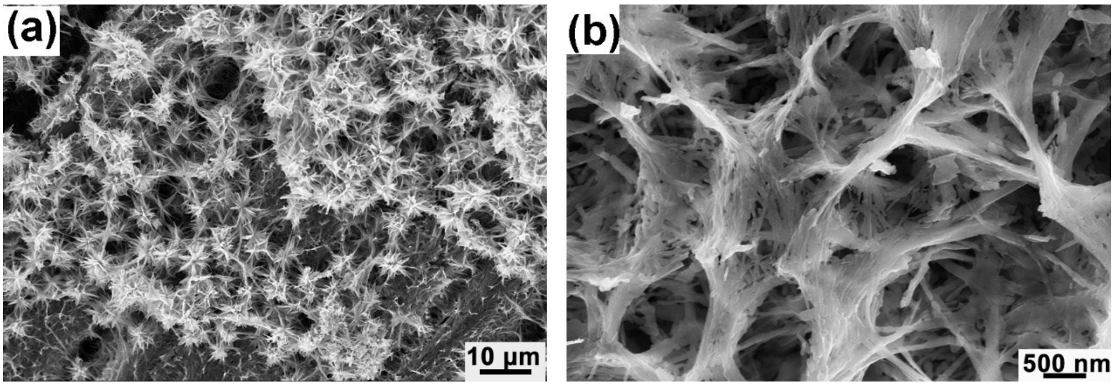

Fig. S19. SEM images of V^{5+}-rich V_6O_{13}/CC cathodes after 1000-cycling test: (a) at a low magnification; (b) at a high magnification.

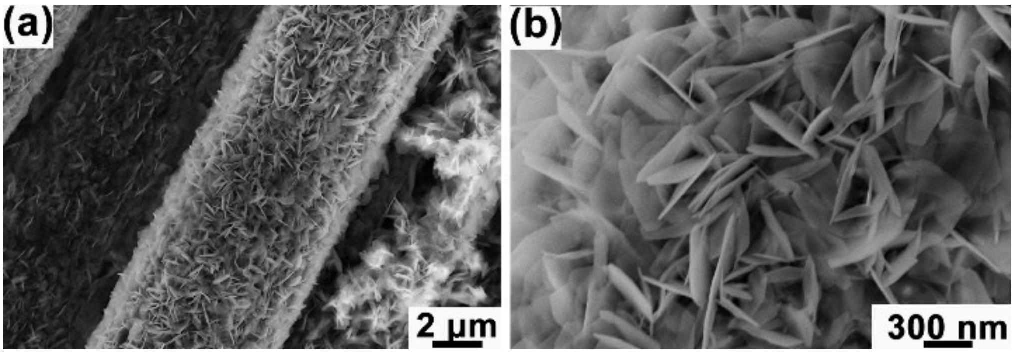

Fig. S20. SEM images of Zn/CC anode after cycling test: (a) at a low magnification; (b) at a high magnification.

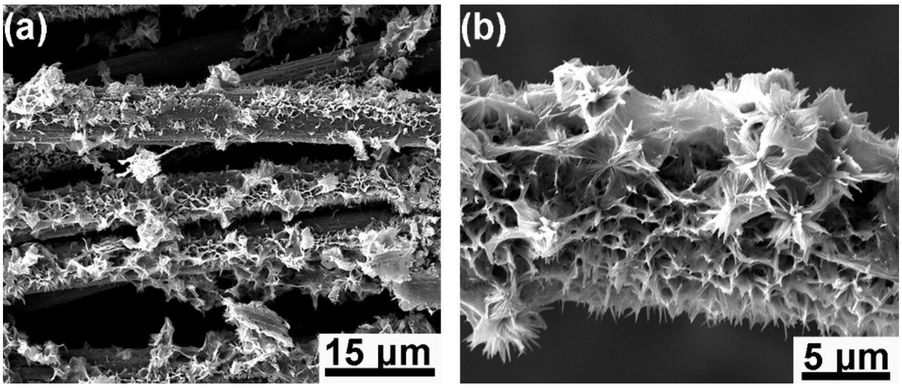

Fig. S21. SEM images of V^{5+}-rich V_6O_{13}/CC cathodes after discharging to 0.2V: (a) at a low magnification; (b) at a high magnification.

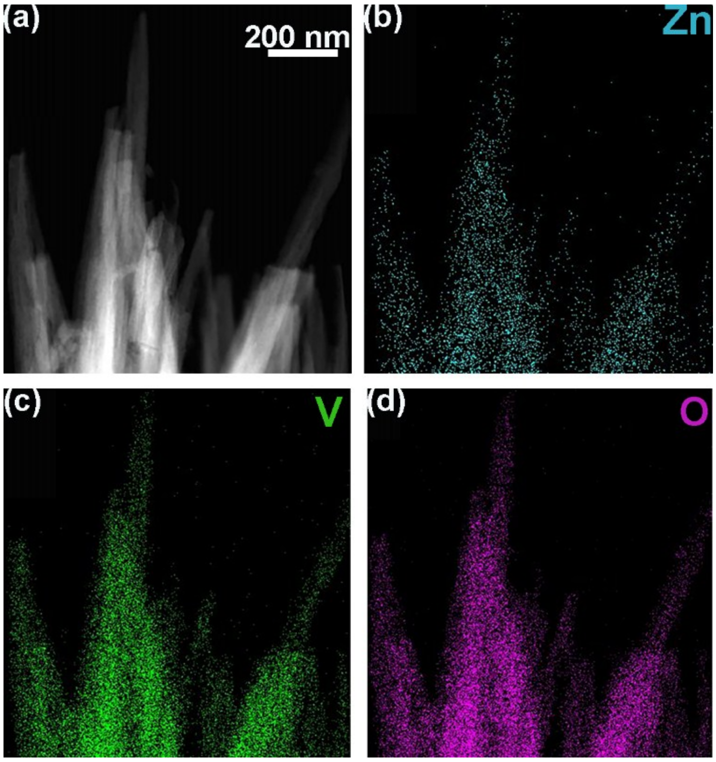

Fig. S22. STEM characterization of V_6O_{13} cathodes after discharging to 0.2V: (a) HADDF image. Elemental mappings of (b) Zn. (c) V. (d) O.

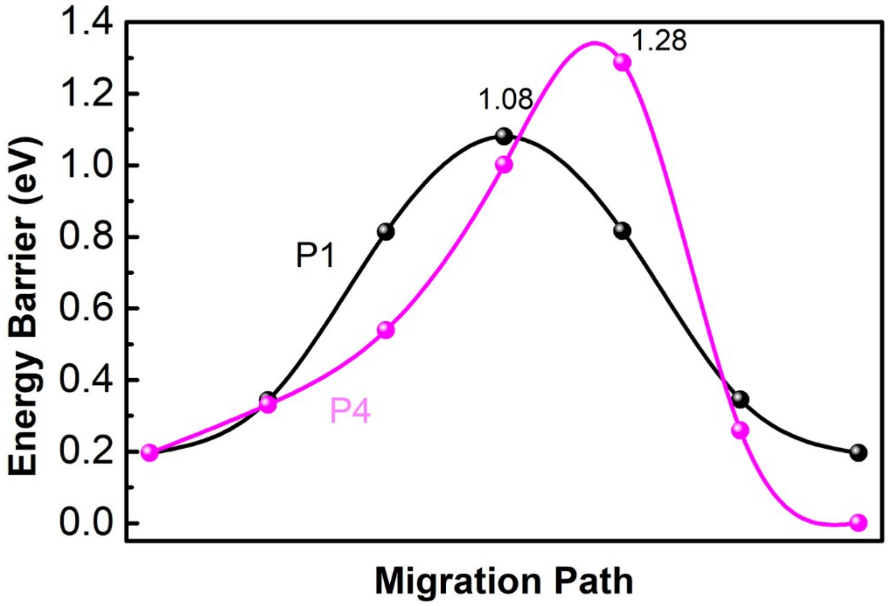

Fig. S23. Calculated diffusion energy barriers for paths P1 and P4.

Table S1. A summary of the electrochemical performance of state-of-the-art V-based cathodes for ZIBs

Materials	Current collector	Electrolyte	Discharge capacity (mAh g^{-1})	Rate capability (mAh g^{-1})	Cyclic stability	Energy density /Power density
$H_2V_3O_8$ nanowires/graphene[1]	Ti foil	3M $Zn(CF_3SO_3)_2$	394 (0.1 A/g)	270 (6 A/g)	87% 2000 cycles	168 Wh kg^{-1} at 34 W kg^{-1}
Utralong $Zn_3V_2O_7(OH)_2{\cdot}2H_2O$ nanowire[2]	Stainless steel	1M $ZnSO_4$	213 (0.05 A/g)	54 (3 A/g)	68% 300 cycles	214 Wh kg^{-1}
VO_2(B) nanofibers[3]	Ti foil	3M $Zn(CF_3SO_3)_2$	357 (0.1 A/g)	171 (51.2 A/g)	50 cycles	297 Wh kg^{-1} at 180 W kg^{-1}
$V_2O_5{\cdot}nH_2O$/graphene[4] (plate-like structure)	Ti foil	3M $Zn(CF_3SO_3)_2$	381 (0.06 A/g)	248 (30 A/g)	71% 900 cycles	144 Wh kg^{-1}
Porous V_2O_5[5]	Ti foil	$Zn(CF_3SO_3)_2$ -LiTFSI	238 (0.05 A/g)	156 (1 A/g)	80% 2000 cycles	/
RGO/VO_2 composite films[6] (porous network)	Stainless steel	3M $Zn(CF_3SO_3)_2$	276 (0.1 A/g)	120 (35 A/g)	99% 1000 cycles	65 Wh kg^{-1} at 7.8 kW kg^{-1}
VO_2 nanorods[7]	-	1M $ZnSO_4$	325.6 (0.05 A/g)	72 (5 A/g)	86% 5000 cycles	/
V_6O_{13} powder[8] (agglomeration of platelets)	Pyrolytic graphite film	3M $Zn(CF_3SO_3)_2$	360 (0.2 A/g)	145 (24 A/g)	92% 2000 cycles	/
$V_6O_{13}{\cdot}nH_2O$ nanosheets[9]	-	3M $Zn(CF_3SO_3)_2$	395 (0.1 A/g)	97 (20 A/g)	87% 1000 cycles	/
$Cu_3(OH)_2V_2O_7{\cdot}2H_2O$ nanosheets[10]	Stainless steel	3M $ZnSO_4$	336 (1 A/g)	-	1000 cycles 160 mAh/g	/
$V_5O_{12}{\cdot}6H_2O$ nanobelt[11]	Stainless steel	3M $Zn(CF_3SO_3)_2$	354.8 (0.5 A/g)	228 (5 A/g)	94% 1000 cycles	194 Wh kg^{-1} at 2.1 kW kg^{-1}
$H_2V_3O_8$ nanowires[12]	Ti foil	3M $Zn(CF_3SO_3)_2$	423.8 (0.1 A/g)	113.9 (5 A/g)	94% 1000 cycles	250 Wh kg^{-1}
$V_3O_7{\cdot}H_2O$[13]	-	1M $ZnSO_4$	375 (0.375 A/g)	270 (3 A/g)	80% 200 cycles	/
$Zn_2V_2O_7$ nanowire[14]	Stainless steel	1M $ZnSO_4$	248 (0.05 A/g)	170 (4.4 A/g)	85% 1000 cycles	90 Wh kg^{-1} at 6.4 kW kg^{-1}
$Na_{0.33}V_2O_5$ nanowire [15]	Ti foil	3M $Zn(CF_3SO_3)_2$	373 (0.2A/g)	96.4 (2 A/g)	93% (1000 cycles)	/
$Ca_{0.25}V_2O_5{\cdot}nH_2O$ nanobelt[16]	-	1M $ZnSO_4$	340 (0.2C)	72 (80 C)	86% 3000 cycles	267 Wh kg^{-1} at 53.4 W kg^{-1}
Bulk V_2O_5[17]	Ti foil	3M $Zn(CF_3SO_3)_2$	470 (0.2A/g)	386 (10 A/g)	91.1% 4000 cycles	274 Wh kg^{-1} at 7.1 kW kg^{-1}

V_2O_5 nanosheet[18]	-	3M $ZnSO_4$	372 (0.3A/g)	-	113mAh/g (400 cycles)	90 Wh kg^{-1} at 6.4 kW kg^{-1}
$V_{10}O_{24}$ nanobelt[19]	graphite paper	3M $Zn(CF_3SO_3)_2$	415 (0.2A/g)	166 (5 A/g)	65% 3000 cycles	/
Al-doped $V_{10}O_{24}$ nanobelt[19]	graphite paper	3M $Zn(CF_3SO_3)_2$	431 (0.2A/g)	232 (5 A/g)	98% 3000 cycles	/
VO_2 nanorod[20]	carbon fibre paper	1M $ZnSO_4$	353 (1A/g)	272 (3 A/g)	75.5% 945 cycles	/
V_2O_5 nanopaper (V_2O_5 nanofiber /carbon nanotubes)[21]	-	2M $ZnSO_4$	375 (0.5A/g)	219 (10 A/g)	77% 500 cycles	/
V_2O_5 hollow spheres[22]	Ti foil	3M $ZnSO_4$	280 (0.2A/g)	108 (10 A/g)	82.5% 6200 cycles	/
V^{4+}-V_2O_5 Hollow nanosphere[23]	Stainless steel	2M $ZnSO_4$	262.1 (1A/g)	124.9 (15 A/g)	140 mAh/g 1000 cycles	/
This work	Carbon cloth (free-standing)	3M $ZnSO_4$	520 (0.5 A/g),	234 (15 A/g)	335 mAh/g 1000 cycles	234 Wh kg^{-1} at 205 W kg^{-1}

References

1 Q. Pang, C. Sun, Y. Yu, K. Zhao, Z. Zhang, P. M. Voyles, G. Chen, Y. Wei and X. Wang, *Adv. Energy Mater.*, 2018, **8**, 1800144.

2 C. Xia, J. Guo, Y. Lei, H. Liang, C. Zhao and H. N. Alshareef, *Adv. Mater.*, 2018, **30**, 1705580.

3 J. Ding, Z. Du, L. Gu, B. Li, L. Wang, S. Wang, Y. Gong and S. Yang, *Adv. Mater.*, 2018, **30**, 1800762.

4 M. Yan, P. He, Y. Chen, S. Wang, Q. Wei, K. Zhao, X. Xu, Q. An, Y. Shuang and Y. Shao, *Adv. Mater.*, 2017, **30**.

5 P. Hu, M. Yan, T. Zhu, X. Wang, X. Wei, J. Li, L. Zhou, Z. Li, L. Chen and L. Mai, *Acs Appl. Mater. Interfaces*, 2017, **9**, 42717.

6 D. Xi, W. Fang, Z. Linlin, C. Hongmei and N. Zhiqiang, *Energy Storage Mater.* 2019, **17**, 143.

7 L. Chen, Y. Ruan, G. Zhang, Q. Wei, Y. Jiang, T. Xiong, P. He, W. Yang, M. Yan and Q. An, *Chem. Mater.*, 2019, **31**, 699-706.

8 J. Shin, D. S. Choi, H. J. Lee, Y. Jung and J. W. Choi, *Adv. Energy Mater.*, 2019, **9**, 1900083.

9 J. Lai, H. Zhu, X. Zhu, H. Koritala and Y. Wang, *ACS Appl. Energy Mater.*, 2019, **2**, 1988-1996.

10 L. Shan, J. Zhou, M. Han, G. Fang, X. Cao, X. Wu and S. Liang, *J. Mater. Chem. A*, 2019, **7**, 7355-7359.

11 N. Zhang, M. Jia, Y. Dong, Y. Wang, J. Xu, Y. Liu, L. Jiao and F. Cheng, *Adv. Funct. Mater.*, 2019, **29**, 1807331.

12 P. He, Y. Quan, X. Xu, M. Yan, W. Yang, Q. An, L. He and L. Mai, *Small*, 2017, **13**, 1702551.

13 D. Kundu, S. H. Vajargah, L. Wan, B. Adams, D. Prendergast and L. F. Nazar, *Energy Environ. Sci.*, 2018, **11**, 881-892.

14 B. Sambandam, V. Soundharrajan, S. Kim, M. H. Alfaruqi, J. Jo, S. Kim, V. Mathew, Y.-k. Sun and J. Kim, *J. Mater. Chem. A*, 2018, **6**, 3850-3856.

15 P. He, G. Zhang, X. Liao, M. Yan, X. Xu, Q. An, J. Liu and L. Mai, *Adv. Energy Mater.*, 2018, **8**, 1702463.

16 C. Xia, J. Guo, P. Li, X. Zhang and H. N. Alshareef, *Angew. Chem. Int. Ed.*, 2018, **57**, 3943-3948.

17 N. Zhang, Y. Dong, M. Jia, X. Bian, Y. Wang, M. Qiu, J. Xu, Y. Liu, L. Jiao and F. Cheng, *ACS Energy Lett.*, 2018, **3**, 1366-1372.

18 Z. Jiang, L. Shan, Z. Wu, G. Xun and S. Liang, *Chem. Commun.*, 2018, **54**, 4457-4460.

19 Q. Li, T. Wei, K. Ma, G. Yang and C. Wang, *ACS Appl. Mater. Interfaces*, 2019, **11**, 20888-20894.

20 Z. Li, S. Ganapathy, Y. Xu, Z. Zhou, M. Sarilar and M. Wagemaker, *Adv. Energy Mater.*, 2019, **9**, 1900237.

21 Y. Li, Z. Huang, P. K. Kalambate, Y. Zhong, Z. Huang, M. Xie, Y. Shen and Y. Huang, *Nano Energy*, 2019, **60**, 752-759.

22 H. Qin, L. Chen, L. Wang, X. Chen and Z. Yang, *Electrochimica Acta*, 2019, **306**, 307-316.

23 F. Liu, Z. Chen, G. Fang, Z. Wang, Y. Cai, B. Tang, J. Zhou and S. Liang, *Nano-Micro Lett.*, 2019, **11**, 25.